The EMBO Journal (2011) 30, 3147–3159 | © 2011 European Molecular Biology Organization | All Rights Reserved 0261-4189/11
www.embojournal.org

THE EMBO JOURNAL

The functions of the actin nucleator Cobl in cellular morphogenesis critically depend on syndapin I

Lukas Schwintzer, Nicole Koch[1], Rashmi Ahuja[1], Julia Grimm, Michael M Kessels* and Britta Qualmann*

Institute for Biochemistry I, Jena University Hospital, Friedrich Schiller University Jena, Jena, Germany

Spatial control of cortical actin nucleation is indispensable for proper establishment and plasticity of cell morphology. Cobl is a novel WH2 domain-based actin nucleator. The cellular coordination of Cobl's nucleation activity, however, has remained elusive. Here, we reveal that Cobl's cellular functions are dependent on syndapin. Cobl/syndapin complexes form *in vivo*, as demonstrated by colocalization, coimmunoprecipitation and subcellular recruitment studies. *In vitro* reconstitutions and subcellular fractionations demonstrate that, via its lipid-binding Fer/CIP4 Homology (FCH)-Bin/Amphiphysin/Rvs (F-BAR) domain, syndapin recruits Cobl to membranes. Consistently, syndapin I RNAi impairs cortical localization of Cobl. Further functional studies in neurons show that Cobl and syndapin I work together in dendritic arbor development. Importantly, both proteins are crucial for dendritogenesis. Cobl-mediated functions in neuromorphogenesis critically rely on syndapin I and interestingly also on Arp3. Endogenous Cobl, syndapin I and the Arp2/3 complex activator and syndapin-binding partner N-WASP were present in one complex, as demonstrated by coimmunoprecipitations. Together, these data provide detailed insights into the molecular basis for Cobl-mediated functions and reveal that different actin nucleators are functionally intertwined by syndapin I during neuromorphogenesis.

The EMBO Journal (2011) **30,** 3147–3159. doi:10.1038/emboj.2011.207; Published online 1 July 2011
Subject Categories: cell & tissue architecture; neuroscience
Keywords: cell cortex; cordon-bleu; cytoskeleton; neuronal cell morphology; N-WASP and Arp2/3 complex-mediated actin nucleation

Introduction

Forces brought about by the actin cytoskeleton associated with the plasma membrane are important for shaping the morphology of defined membrane areas and of entire cells. Drastic alterations of cell morphology, which are based on coordinated functions of the actin cytoskeleton and microtubules, are required during neuromorphogenesis and neuronal network formation in the brain (Conde and Cáceres, 2009; Kessels *et al*, 2010).

Of outmost importance for all cytoskeletal processes is a tight control of filament formation in time and space. For actin filament formation, the rate-limiting step *in vitro* is the assembly of a trimeric actin nucleus onto which further actin monomers can then add spontaneously. Despite the plethora of actin structures found in different cells, only a very limited number of actin-nucleating machines are well established, mainly the Arp2/3 complex and the formin family. Recently, with Spire, Cobl, leiomodin and JMY, a group of novel actin nucleators has been discovered (Chesarone and Goode, 2009; Qualmann and Kessels, 2009). Spire/formin complexes (Quinlan *et al*, 2005, 2007), Cobl (Ahuja *et al*, 2007), leiomodin2 (Chereau *et al*, 2008) and the nuclear p53 cofactor JMY (Zuchero *et al*, 2009) all use Wiskott–Aldrich homology 2 (WH2) domains for actin binding. Domain organization and first mechanistic studies of these novel nucleators suggest that, despite their common use of WH2 domains, they may employ very different molecular mechanisms to promote actin filament formation (Qualmann and Kessels, 2009). Cobl uses three C-terminal WH2 domains for actin binding and formation of non-bundled, unbranched filaments (Ahuja *et al*, 2007).

The *in vivo* functions of these novel nucleators, however, are only emerging, as analyses of endogenous proteins, loss-of-function studies and also knowledge of interactions of these WH2 domain-based nucleators with cellular components besides actin are still sparse.

Here, we reveal that the actin nucleator Cobl, which has been demonstrated to have a critical role in dendrite formation and dendritic arborisation (Ahuja *et al*, 2007), implements its functions in neuromorphogenesis by direct complex formation with a member of the syndapin/PACSIN family of Fer/CIP4 Homology (FCH)-Bin/Amphiphysin/Rvs (F-BAR) domain proteins (Kessels and Qualmann, 2004; Fütterer and Machesky, 2007; Frost *et al*, 2008; Aspenström, 2009), the brain-enriched and plasma membrane-interacting protein syndapin I.

Results

The N-terminal Cobl homology domain of Cobl interacts with syndapin I, II and III in vitro

The molecular mechanisms, by which the actin nucleator Cobl achieves its cell biological functions, are largely unclear. We have identified Cobl in a yeast two-hybrid screen for Arp2/3 complex-independent actin filament formation-promoting factors interacting with syndapin I (Ahuja *et al*, 2007). In addition to three C-terminal WH2 domains, the presence of the linker region L2 between the second and third WH2 domain was of importance for Cobl-mediated actin nuclea-

*Corresponding authors. MM Kessels or B Qualmann, Institute for Biochemistry I, Jena University Hospital, Friedrich Schiller University Jena, Nonnenplan 2-4, Jena 07743, Germany.
Tel.: +49 3641 9 38120; Fax: +49 3641 9 396 302;
E-mail: michael.kessels@mti.uni-jena.de or
Tel.: +49 3641 9 396 300; Fax: +49 3641 9 396 302;
E-mail: britta.qualmann@mti.uni-jena.de
[1]These authors contributed equally to this work

Received: 22 December 2010; accepted: 3 June 2011; published online: 1 July 2011

tion (Ahuja *et al*, 2007). Since the linker L2 is proline-rich, we speculated that syndapin I may interact with the linker L2 and thereby directly interface with Cobl. To test this, we conducted coprecipitation experiments with GFP–Cobl fusion proteins expressed in HEK293 cells (Figure 1A) and immobilized GST-syndapin I. Surprisingly, the actin-nucleating C-terminus of Cobl (Cobl-CT; Cobl 1176–1337) remained in the supernatant and did not associate with syndapin I (Figure 1B–D).

Whereas also none of the more central parts of Cobl associated with syndapin I, an N-terminal part of Cobl, which represents a thus far uncharacterized, so-called Cobl homology domain (Pfam Database accession, PF09469), Cobl 1–408, very efficiently interacted with syndapin I (Figure 1B–D).

Coprecipitation analyses with syndapin deletion and point mutants, respectively, revealed that the C-terminal Src homology 3 (SH3) domain of syndapin I is critical and sufficient for the interaction with Cobl (Figure 1E–G).

In mammals, the syndapin family is encoded by three different genes. All three isoforms are expressed in the brain and show particularly high sequence conservation in the SH3 domain (Kessels and Qualmann, 2004). In line with this, syndapin I, syndapin II and syndapin III were all able to efficiently interact with Cobl 1–408 *in vitro* (Figure 1H–J).

Cobl/syndapin protein complexes are formed in vivo

In order to address whether the Cobl/syndapin interaction also occurs *in vivo*, we conducted coimmunoprecipitation studies. Coimmunoprecipitation of GFP–Cobl 1–408 with Flag-syndapin I overexpressed in HEK293 cells indeed demonstrated complex formation of both proteins *in vivo*. Since neither coexpressed GFP was precipitated nor any syndapin I or Cobl proteins were found in immunoprecipitates of unrelated IgGs, the coimmunoprecipitations of GFP–Cobl 1–408 were highly specific (Figure 2A–D).

Similar results were obtained with GFP–Cobl constructs and a Flag-tagged version of syndapin II, the ubiquitously expressed syndapin isoform (Supplementary Figure S1). Cobl can thus interact with both syndapin I and II in cellular extracts.

In order to be able to detect putative endogenous syndapin/Cobl complexes in brain, we raised antibodies against Cobl 175–324 (ARA) and 750–1005 (DBY). Antibodies from both sera were affinity-purified and proved applicable in immunofluorescence microscopy and western blotting (Supplementary Figure S2).

The use of the anti-Cobl antibodies in analyses of anti-syndapin I immunoprecipitates from rat brain extracts revealed a specific coimmunoprecipitation of endogenous Cobl together with endogenous syndapin I and thus demonstrated the existence of Cobl/syndapin protein complexes in the brain (Figure 2E–H).

Cobl and syndapin I show spatial overlap in developing and mature neurons

Subsequent colocalization studies aimed at obtaining first hints on whether Cobl and syndapin I may work together in controlling neuromorphogenesis. In dissociated primary hippocampal neurons kept in culture for 2 days (days *in vitro* (DIV) 2), Cobl was present in the entire cells with accumulations in the cell body and in growth cones, as previously described (Ahuja *et al*, 2007). Syndapin I immunostaining

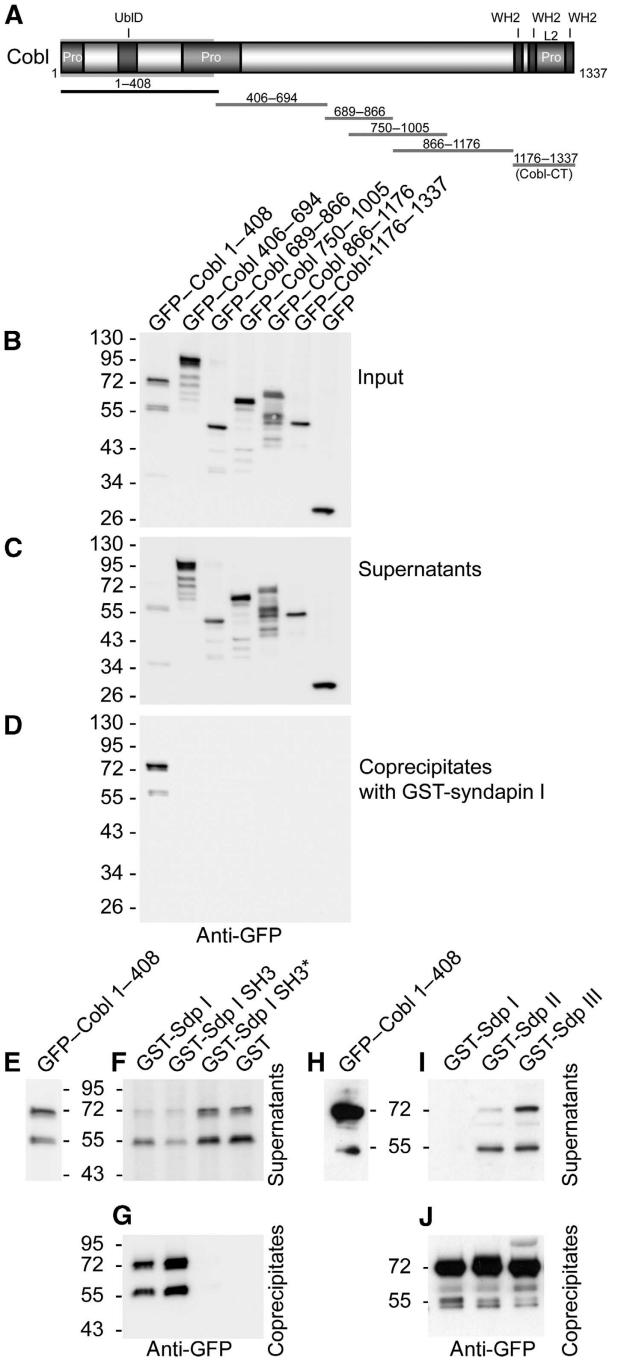

Figure 1 Syndapins associate with the N-terminal region of Cobl via their SH3 domain. (**A**) Schematic representation of the murine Cobl protein showing its PRDs (Pro), an Ubiquitin-like fold domain (UblD; DOI:10.2210/pdb2daj/pdb), the N-terminal Cobl homology domain (Pfam Database accession number PF09469; grey frame) and the three C-terminal WH2 domains. Additionally, Cobl fragments used for the analyses of syndapin-binding regions are depicted (black, syndapin-binding; grey not binding). (**B–I**) Verification and characterization of Cobl/syndapin interactions by coprecipitation analyses. (**B–D**) Syndapin I associates with the N-terminal third of Cobl, as demonstrated by anti-GFP immunoblot analyses of coprecipitations of GFP–Cobl fragments and GFP from HEK293 cells lysates with GST-syndapin I. (**E–G**) Immobilized GST-syndapin I full-length and GST-syndapin I SH3 domain but not GST and a mutant unable to interact with proline-rich motifs (Sdp I SH3*, P434L) precipitate GFP-tagged Cobl 1–408 (**F**, **G**). (**H–J**) GFP–Cobl 1–408 was efficiently precipitated by all three isoforms of the syndapin family.

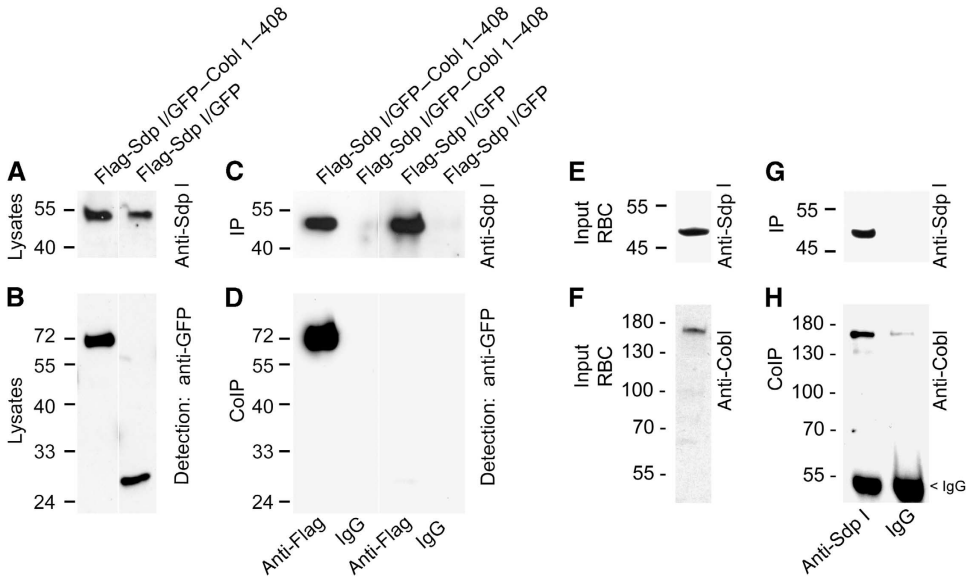

Figure 2 Coimmunoprecipitation of heterologous and of endogenous proteins demonstrate that complexes of Cobl and syndapin I are formed *in vivo*. (**A**–**D**) Heterologous coimmunoprecipitations. Immunoblot analyses with anti-syndapin I and anti-GFP antibodies revealed that Flag-syndapin I was immunoprecipitated by immobilized anti-Flag antibodies but not by unrelated IgGs (**C**) and that GFP–Cobl 1–408 but not GFP was specifically coimmunoprecipitated with syndapin I (**D**). White lines indicate a sample omitted from the blots. (**E**–**H**) Endogenous Cobl and syndapin I were coimmunoprecipitated from rat brain extracts. Cobl and syndapin I were detected in rat brain extracts (RBC) using guinea pig anti-syndapin I and rabbit anti-Cobl (ARA^{rb}) antibodies, respectively (**E**, **F**; Input). Syndapin I was specifically immunoprecipitated by immobilized rabbit anti-syndapin I antibodies, as detected by guinea pig anti-syndapin I antibodies (**G**; IP). Anti-Cobl immunoblot analyses of immunoprecipitates revealed a specific coimmunoprecipitation of Cobl with syndapin I (**H**; CoIP).

showed a very similar pattern (Figure 3A–C). Also in DIV21 neurons, Cobl and syndapin I colocalized. Both proteins showed enrichments in perinuclear areas and in discrete puncta along the neurites (Figure 3D–F, and high-magnification insets). In line with these observations, syndapin I has been reported to be present in synapses (Qualmann *et al*, 1999; Pérez-Otāno *et al*, 2006).

Immunohistological analyses showed that Cobl is enriched in the dentate gyrus and in the different areas of the hippocampus (Supplementary Figure S3). Parallel control incubations without primary antibodies (not shown), with non-immune IgGs (not shown) and with unrelated antibodies affinity purified from the same antisera as the anti-Cobl antibodies employed (for characterization of these antibodies see Supplementary Figure S2), that were imaged in parallel to hippocampal sections stained with affinity-purified anti-Cobl antibodies, demonstrated that the anti-Cobl immunolabelling was specific (Supplementary Figure S3).

Analyses of the syndapin distribution in the brain with antibodies specific for syndapin I (Qualmann *et al*, 1999; Braun *et al*, 2005) also revealed a presence of syndapin I in neurons of the hippocampus (not shown). At higher resolution, syndapin I and Cobl particularly localized in the perikarya and in the dendritic trees of hippocampal pyramidal cells (Figure 3G–I). Taken together, Cobl and syndapin I show spatial overlap in the brain.

Syndapin I and Cobl work together in dendritogenesis

The Cobl/syndapin I protein interaction and the spatial overlap of the expression and localization of both proteins in the brain and in dissociated neuronal cultures, respectively, suggested that Cobl and syndapin I may have common functions. Overexpression of Cobl and syndapin I in hippocampal neurons both lead to an increase in the number of dendrites (+17% each) and of dendritic branch points (+47 and +37%, respectively) compared with control cells (Figure 4A–F, I and J). Interestingly, coexpression of Cobl and syndapin I resulted in even stronger phenotypes (Figure 4G–J).

Syndapin I directly interacts with the three highly conserved motifs characteristic for the Cobl homology domain

The observation that Cobl and syndapin I coexpression led to a further enhancement of dendritic branch formation raised the question how a putative cofunction of syndapin I and Cobl could be brought about mechanistically. We reasoned that syndapin I may promote Cobl's functions in dendritogenesis by recruiting Cobl to the cell cortex. This would imply (i) that syndapin binds to Cobl directly, (ii) that the interactions in syndapin/Cobl complexes are strong enough to dictate the (re)localization of a binding partner *in vivo* and (iii) that indeed such complexes of syndapin and Cobl associate with the membrane. If all these scenarios are correct, then finally, it should (iv) be possible to detect subpools of both endogenous syndapin I and endogenous Cobl, which are associated with the plasma membrane, and (v) maybe even reveal an impairment of Cobl's cortical localization upon syndapin deficiency. We thus next addressed all these points experimentally.

Further dissection of the N-terminal region of Cobl comprising the syndapin-binding Cobl homology domain (Figure 5A) showed that syndapin I associates with the first proline-rich domain (PRD) (aa 1–47) and with the N-terminal part of the second PRD of Cobl (aa 319–396), whereas the region between the two PRDs did not associate with syndapin. Interestingly, breaking the Cobl 319–396 interface into

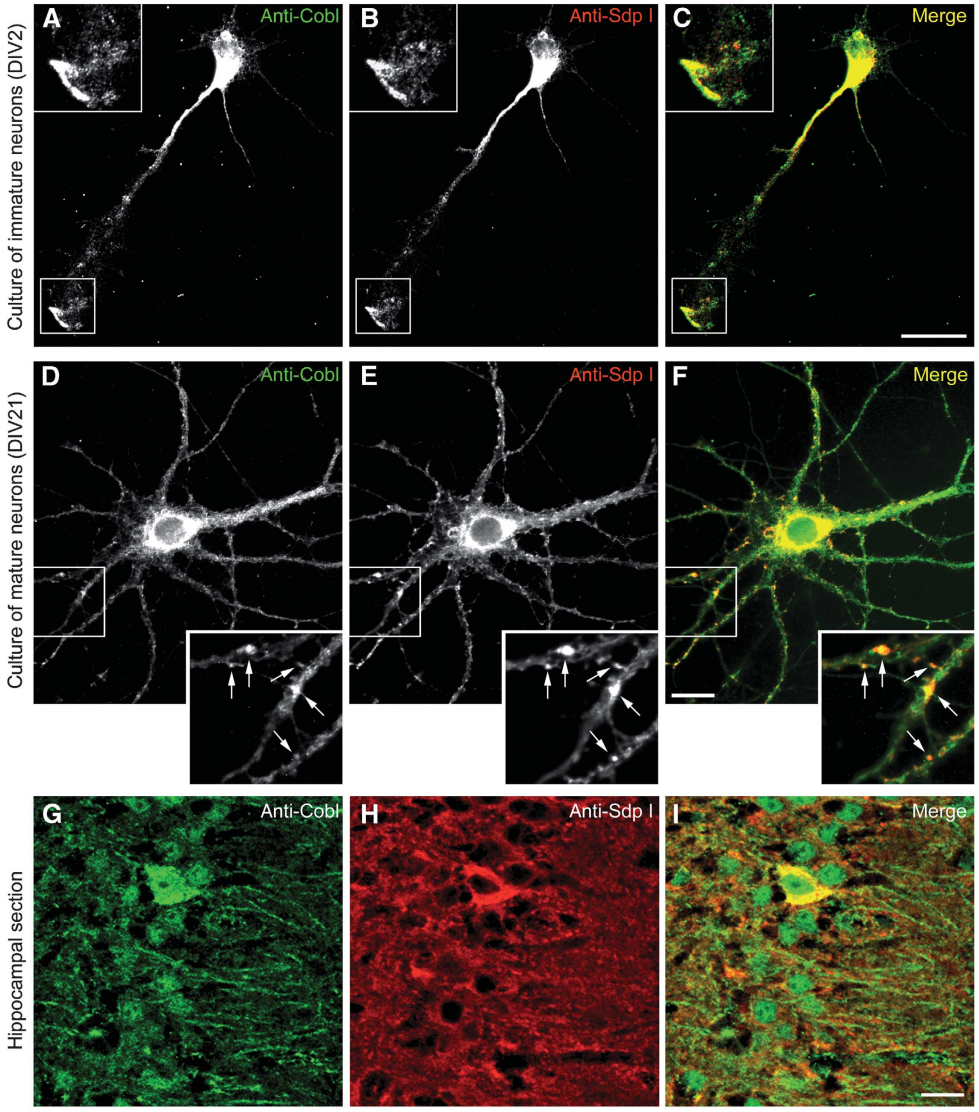

Figure 3 Colocalization of endogenous Cobl and syndapin I in primary neuronal cultures and in hippocampal brain sections. Primary hippocampal neurons kept in culture for 2 days (**A**–**C**) and mature primary hippocampal neurons kept in culture for 21 days (**D**–**F**) were stained with rabbit anti-Cobl antibodies (ARA^{rb}) (**A**, **D**; green in merge) and guinea pig anti-syndapin I antibodies (**B**, **E**; red in merge) (PFA fixation). The merged images (**C**, **F**) show colocalization in the cell bodies, growth cones (**C**) and in punctuate areas located in the neurites of mature neurons (**F**; arrows on enlarged insets). (**G**–**I**) Adult mouse brain sections immunostained for Cobl (**G**; anti-Cobl DBY^{rb}) and syndapin I (**H**; guinea pig anti-syndapin **I**). Merged image (**I**) shows the colocalization of both proteins in the cell bodies and dendritic trees of hippocampal pyramidal cells. Bars, 25 μm.

Cobl 319–360 and Cobl 355–396 strongly suggested that syndapin I has at least two binding sites in this region, that is together with the SH3 domain binding motif in Cobl 1–47 in total at least three (Figure 5B–D).

To address which syndapin-binding regions mediate interaction *in vivo*, we conducted coimmunoprecipitation studies with Flag-syndapin I and with coexpressed GFP–Cobl 1–324 and GFP–Cobl 319–396, respectively. Both Cobl fragments were specifically coimmunoprecipitated with Flag-syndapin I (Figure 5E–H). These data showed that complex formation of syndapin I and Cobl *in vivo* occurs with the N-terminal site and with more central sites and that association furthermore does not rely on the presence of all three regions but that minimally one of the binding regions, as in Cobl 1–324, is sufficient for interaction *in vivo*.

Two partially overlapping PxxP-motifs are present in Cobl 1–47. Several PxxP-motifs are present in Cobl 319–360 and Cobl 355–396 (Figure 5I; Supplementary Figure S4). *In silico* analyses identified a class I motif of similar sequence in all three segments. The sequence of these three motifs is KrRAPpPP (Figure 5I). Importantly, comparisons of Cobl proteins from a variety of species show that these motifs are conserved in evolution, whereas the flanking sequences show low or no conservation (Supplementary Figure S4).

To firmly prove that the three PxxP-motifs located C-terminal of the third KrRAPpPP-motif are not involved in syndapin-binding, we tested Cobl 54–450Δ323–366 and Cobl 367–713. Both deletion mutants did not associate with the syndapin SH3 domain (Figure 5J–L).

To explicitly prove that all three identified, conserved KrRAPpPP-motifs are the binding sites of the syndapin SH3 domain, we conducted coprecipitation analyses with short peptide sequences comprising the individual KrRAPpPP-motifs. Immobilized syndapin I SH3 domain specifically (GST

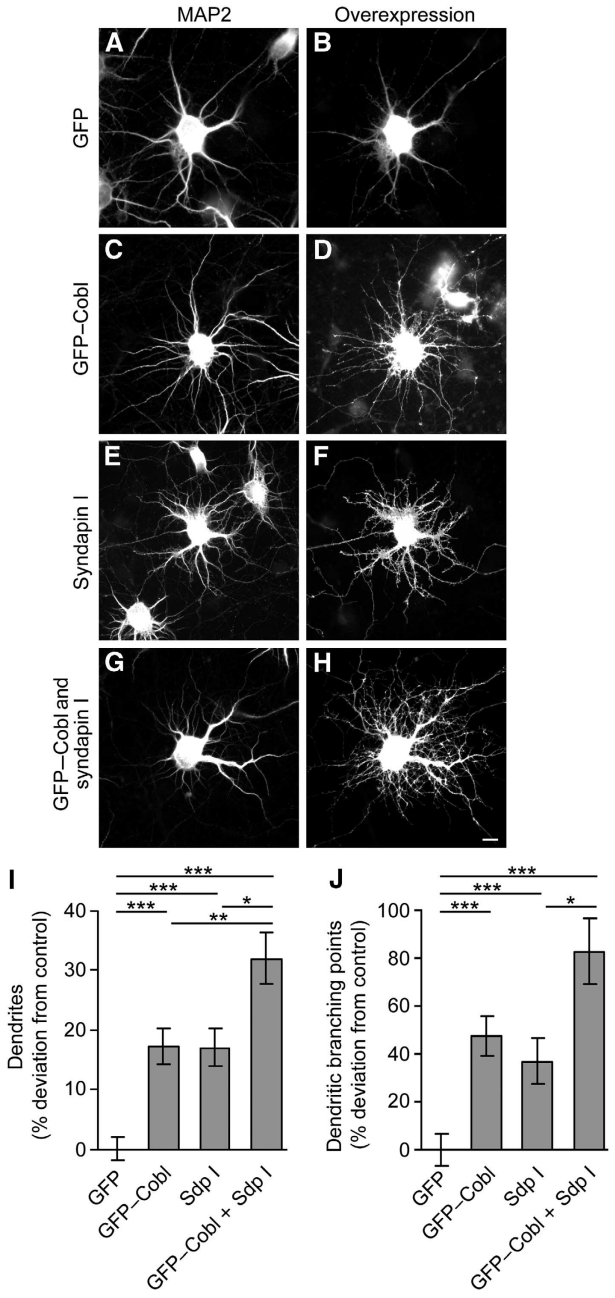

Figure 4 Cobl and syndapin I both function in the control of neuromorphogenesis. (**A**–**H**) At DIV4, primary hippocampal neurons were transfected as indicated and processed for immunofluorescence microscopy 2 days later. Immunostainings of MAP2 were used for quantitative determination of the morphology of transfected neurons (**A**, **C**, **E**, **G**). Primary hippocampal neurons overexpressing GFP–Cobl (**C**, **D**) and Flag-syndapin I (**E**, **F**), respectively, showed an increase in dendrite number and branching when compared with control cells expressing GFP (**A**, **B**). Cooverexpression of GFP–Cobl and syndapin I enhanced dendrite branching even further (**G**, **H**). Image in (**H**) shows the syndapin I staining. Scale bar, 10 μm. (**I**, **J**) Quantitative examinations of dendrite number (**I**) and of dendritic branch points (**J**). Data represent mean ± s.e.m. GFP, $n = 220$; GFP–Cobl, $n = 128$; Sdp I, $n = 112$; GFP–Cobl and Sdp I, $n = 77$. $^{*}P < 0.05$; $^{**}P < 0.01$; $^{***}P < 0.001$ (ANOVA and HSD).

controls not shown) and effectively coprecipitated all three KrRAPpPP-motifs of Cobl (Cobl 14–26, GRKM**KARAPPPP**G; Cobl 318–332, MKSDMK**KRRAPPPP**S; Cobl 354–367, QKK**KRRAPAPP**PPQ) (Figure 5M–O).

The next question raised was whether syndapin I is a major binding partner associating with the KrRAPpPP-motifs defining the Cobl homology domain. In order to address this, we conducted precipitation experiments with GST-KrRAPpPP-motif #2 and rat brain extracts and analysed the bound material by SDS–PAGE and Coomassie staining (Figure 5P–R). Interestingly, only one major band was obtained (Figure 5Q). Further detectable protein traces seemed to represent unspecific interactions, as they were also seen either in GST controls (Figure 5P) or in experiments without brain extract (Figure 5Q). The major and specific band had the size of syndapin I (~53 kDa) and was immunopositive for syndapin I antibodies in western blotting experiments (Figure 5R).

Finally, to prove that Cobl/syndapin interactions are indeed direct, we performed blot overlay assays using syndapin I, syndapin II and syndapin III as probes. Both Cobl 1–408 and Cobl 319–470 separated on the blots were specifically detected by all three syndapins used (Figure 5S–W).

Complexes of syndapin I and Cobl bind to lipid surfaces

The finding that Cobl/syndapin interactions are direct allowed for a reconstitution of these complexes to test the hypothesis that such complexes associate with lipid surfaces. For such reconstitutions, GFP–Cobl 1–713 was isolated from HEK293 cells via complex formation with purified GST-syndapin I expressed in *Escherichia coli*. Protein complexes were eluted and added to liposomes made from purified lipids. Then this mixture was subjected to density gradient centrifugation. The majority of the Cobl/syndapin I complexes floated up together with the liposomes in fraction 2 (Figure 6A; black arrowhead). Syndapin I showed a similar liposome interaction when added alone and this interaction was dependent on the N-terminal F-BAR domain (Itoh *et al*, 2005; Dharmalingam *et al*, 2009; data not shown).

Importantly, complexes formed between GST-syndapin I SH3 (i.e. of a deletion mutant lacking the lipid-binding F-BAR domain) and GFP–Cobl 1–713 did not lead to a redistribution of the complex by cofloatation with the liposomes. Instead, the majority of both Cobl and syndapin SH3 stayed at the bottom of the gradient (Figure 6B; grey arrowheads). Further controls, such as GST and GST-syndapin I/GFP (data not shown) also showed that the Cobl recruitment to the membrane fraction is specific and syndapin-dependent.

Quantitative analyses of blots from four different experiments clearly show that the association of Cobl with lipid surfaces is dependent on the lipid-binding syndapin I F-BAR domain. In all, 76 ± 6% of Cobl floated up with the liposomes, when syndapin I was present, while only 5 ± 2% of the Cobl protein did so in control experiments with syndapin deletion mutants lacking the F-BAR domain (Sdp I SH3) (Figure 6C).

Together, these data show that syndapin I is able to recruit Cobl to membranes by direct Cobl/syndapin interactions and that this requires both the lipid-binding F-BAR domain of syndapin I and the Cobl-associating SH3 domain of syndapin I.

Constitutive anchoring of syndapin I at cellular membranes recruits Cobl

Next, it was crucial to demonstrate that syndapin I can not only recruit Cobl in *in vitro* experiments but that syndapin I also has the ability to recruit Cobl *in vivo*. In order to do so,

we used syndapin fusion proteins that were targeted to the outer membrane of mitochondria in a way that they faced the cytosol (mito-syndapin I) and cotransfected GFP–Cobl, GFP–Cobl 1–408 and GFP, respectively. Both Cobl full-length and Cobl 1–408 (Figure 7A–H) as well as GFP–Cobl 1–324 and GFP–Cobl 319–396 (Supplementary Figure S5A–H) were effectively recruited to the mitochondrial membrane surfaces covered with syndapin I. These data also exclude the theoretical possibility that the Cobl/syndapin interaction observed in the coprecipitation and coimmunoprecipitation studies is based on post-solubilization artefacts. The specificity and syndapin I dependence of the recruitment can be concluded from the observations that GFP did not localize to syndapin I-coated mitochondria (Supplementary Figure S5I–L)

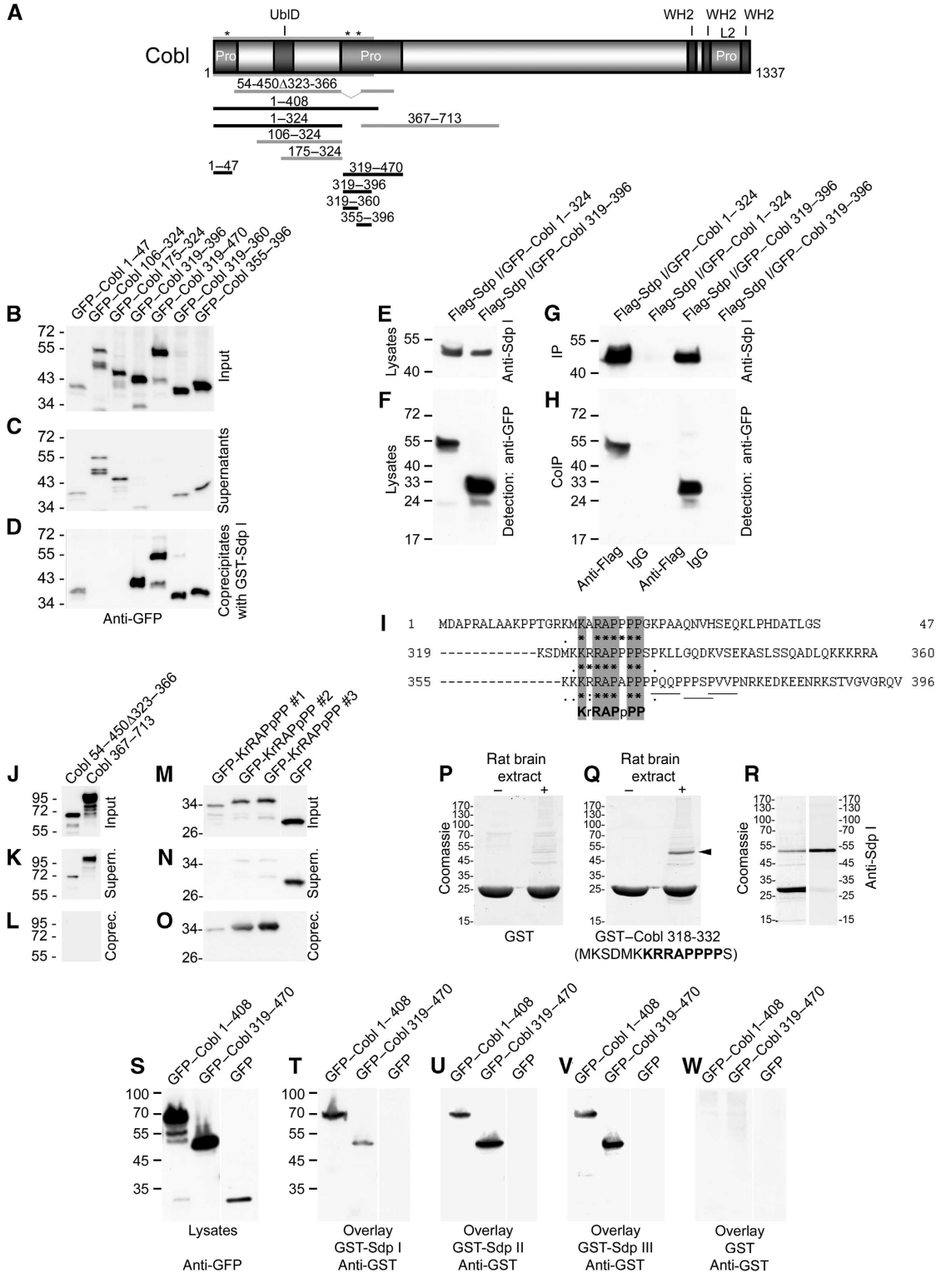

and that, without mito-syndapin I coexpressed, no colocalization with mitochondria (highlighted by mito-Tracker) was observed for full-length Cobl or Cobl 1–408. Instead, these proteins were distributed in the cytosol and exhibited accumulations at the F-actin-rich cell cortex (Cobl full-length; Figure 7I–K) and in the nucleus (Cobl 1–408; Figure 7L–N), respectively.

A subpool of endogenous Cobl and syndapin I is associated with the plasma membrane

We next examined whether a subpool of the endogenous proteins can be detected in association with the plasma membrane. Fractionation and density gradient floatation experiments with rat brain extracts showed that indeed a significant subpool of both the endogenous Cobl protein and the endogenous syndapin I was floating. A majority of Cobl and syndapin I floated from the start fractions 11/12 up to the density gradient fractions 4–6 containing plasma membrane-associated material (Kretzschmar *et al*, 1996), as also confirmed by detection of the integral plasma membrane protein IRTK (Figure 7O–Q).

Immunofluorescence analyses of methanol-fixed primary hippocampal neurons transfected with plasma membrane-targeted GFP (PM-GFP) (Kessels and Qualmann, 2006) showed a colocalization of endogenous Cobl and PM-GFP (Figure 7R–T). This directly visualized cortical Cobl in neurons.

Localization of Cobl to the cell cortex of primary hippocampal neurons depends on syndapin I

Finally, we addressed whether the observed ability of syndapin I to recruit Cobl to membranes is of functional importance *in vivo*. RNAi-mediated knockdown of syndapin I indeed reduced cortical Cobl labelling in comparison to cells transfected with $pRNAT^{PM\text{-}GFP}$ (Figure 7U and V) and untransfected control cells (Figure 7V). Plotting the anti-Cobl signal intensities across the cells clearly showed the reduction in cortical signal (Figure 7W–Y). The ratio of the signal averages of cortical and internal anti-Cobl signals revealed a significant reduction of cortical Cobl localization upon reduction of syndapin I levels (4.25 ± 0.29 versus 3.35 ± 0.11, $P < 0.001$; Figure 7Y). Thus, the cortical localization of Cobl relies on its lipid-binding interaction partner syndapin I.

Syndapin I loss-of-function phenocopies the reduction in dendrite number observed in Cobl-deficient cells

Cobl has been shown to have an important role in dendritogenesis. Cobl-deficient cells exhibited fewer dendritic branches and had ~12% fewer dendrites than control cells

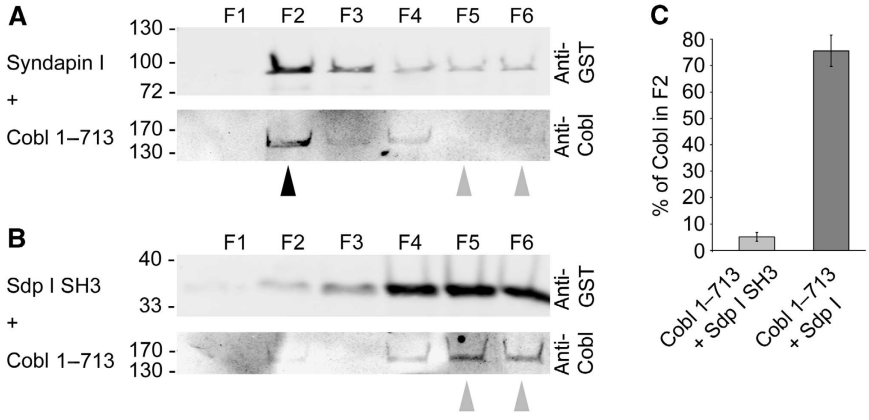

Figure 6 Cobl/syndapin I complexes associate with lipids in a F-BAR domain-dependent manner. Recombinant, purified GST-syndapin I and syndapin I SH3 domain, respectively, were used to purify GFP–Cobl 1–713. These protein complexes were eluted, incubated with liposomes and subjected to density gradient analyses. Immunoblotting of gradient fractions F1–6 shows that, in the presence of syndapin I, Cobl floats with the liposomes (F2) (**A**; black arrowhead), whereas Cobl/syndapin SH3 domain complexes do not float but stay at the bottom of the gradient (F5 and 6) (**B**; grey arrowheads). (**C**) Quantitative analyses of the amount of Cobl detected in the liposome fraction F2. $n = 4$ each. Errors represent s.e.m.

Figure 5 Syndapin I directly interacts with three conserved KrRAPpPP-motifs in the Cobl sequence. (**A**) Schematic representation of the murine Cobl protein and of Cobl fragments used (related to scheme in Figure 1). Asterisks mark positions of KrRAPpPP-motifs. (**B**–**D**) Coprecipitation experiments with immobilized GST-syndapin I and a variety of GFP–Cobl fragments expressed in HEK293 cells analysed by anti-GFP immunoblotting. (**E**–**H**) Heterologous coimmunoprecipitations of Flag-syndapin I with GFP-tagged Cobl 1–324 and GFP–Cobl 319–396. (**I**) Alignment of the three small, syndapin I-associating regions of Cobl identified in (**D**) reveals a consensus motif (KrRAPpPP, conserved residues in bold and shaded). Alternative PxxP-motifs distinct from the three KrRAPpPP-motifs are underlined. (**J**–**O**) Coprecipitation experiments with immobilized GST-syndapin I SH3. GFP–Cobl deletion mutants prove that the alternative PxxP-motifs marked in (**I**) do not bind (**J**–**L**). In contrast, all three GFP-KrRAPpPP-motifs bind to syndapin I individually (**M**–**O**). Shown are lysates (**J**, **M**), supernatants (**K**, **N**) and eluates (**L**, **O**) immunoblotted with anti-GFP antibodies. In (**M**), the GFP lane was moved to the right of the blot image for consistence with (**N**, **O**) (white line). (**P**–**Q**) Affinity purification of brain proteins associating with GST-KrRAPpPP-motifs (#2 shown as example), as detected by Coomassie staining. Immobilized GST and incubations without rat brain cytosol were used as negative controls. (**R**) Analysis of the major band obtained (arrowhead in (**Q**)). One preparative lane was divided for Coomassie staining and anti-syndapin I immunoblotting, respectively. (**S**–**W**) Blot overlay studies. GFP–Cobl fusion proteins and GFP expressed in HEK293 cells were blotted and detected either with anti-GFP antibodies (**S**) or with GST-syndapin I (**T**), GST-syndapin II (**U**), GST-syndapin III (**V**), and GST (**W**; negative control) and subsequent incubation with anti-GST antibodies; one sample on each blot was omitted (white line).

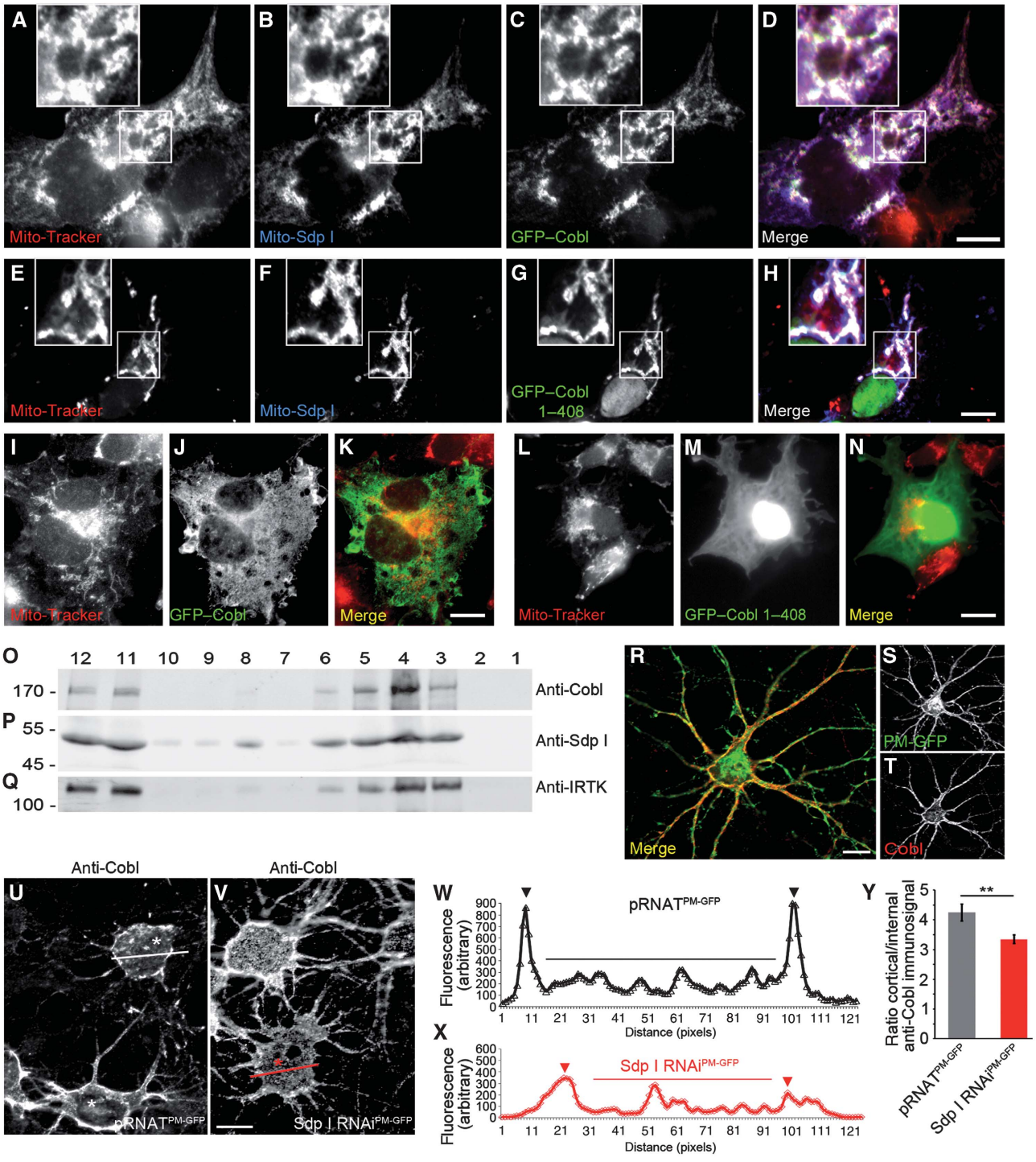

Figure 7 Cortical association of Cobl and its dependence on syndapin I. (**A**–**N**) Constitutively membrane-associated syndapin I recruits GFP–Cobl fusion proteins in intact COS-7 cells. Mitochondria-targeted syndapin I (Mito-Sdp I) (**B**, **F**; blue in merge) was cotransfected together with GFP–Cobl (**C**; green in merge) and GFP–Cobl 1–408 (**G**; green in merge), respectively. Mitochondria were visualized using Mito-Tracker^{TM} (**A**, **E**, **I**, **L**; red in merge). GFP–Cobl and GFP–Cobl 1–408 were recruited to mitochondria-targeted syndapin I (**D**, **H**), whereas they were not when transfected alone (**K**, **N**). Scale bars (**A**–**N**), 20 μm. (**O**–**Q**) Plasma membrane analyses according to Kretzschmar *et al* (1996). S1 fractions of rat cerebrum were subjected to density gradient centrifugation. Immunoblotting of gradient fractions (1, top; 12, bottom) with anti-Cobl and anti-syndapin I antibodies revealed that both endogenous Cobl (**O**) as well as syndapin I (**P**) float to the plasma membrane-containing fractions (fractions 4–6), as verified by immunoblotting for the integral plasma membrane protein IRTK (**Q**). (**R**–**T**) Localization of endogenous Cobl to the PM-GFP-marked cell cortices of DIV7 primary hippocampal neurons transfected with pRNAT$^{PM\text{-}GFP}$ at DIV6 (methanol fixation). (**U**–**Y**) Quantitative evaluation of Cobl's cortical localization in dependence on syndapin I. Profiles of anti-Cobl immunofluorescence intensities across cells transfected with pRNAT$^{PM\text{-}GFP}$ (white asterisks in (**U**)) and with syndapin I RNAi$^{PM\text{-}GFP}$ (red asterisk in (**V**)), respectively, were analysed (**W**, **X**) and the ratios of the averaged maxima of the cortical peaks (marked by arrowheads in (**W**, **X**)) divided by the cytosolic signal (marked by lines in (**W**, **X**)) were compared to exclude varying labelling intensities (**Y**). $n = 47$ and 50. Bars in (**T**, **V**), 10 μm. Errors represent s.e.m. $^{**}P < 0.01$ (*t*-test).

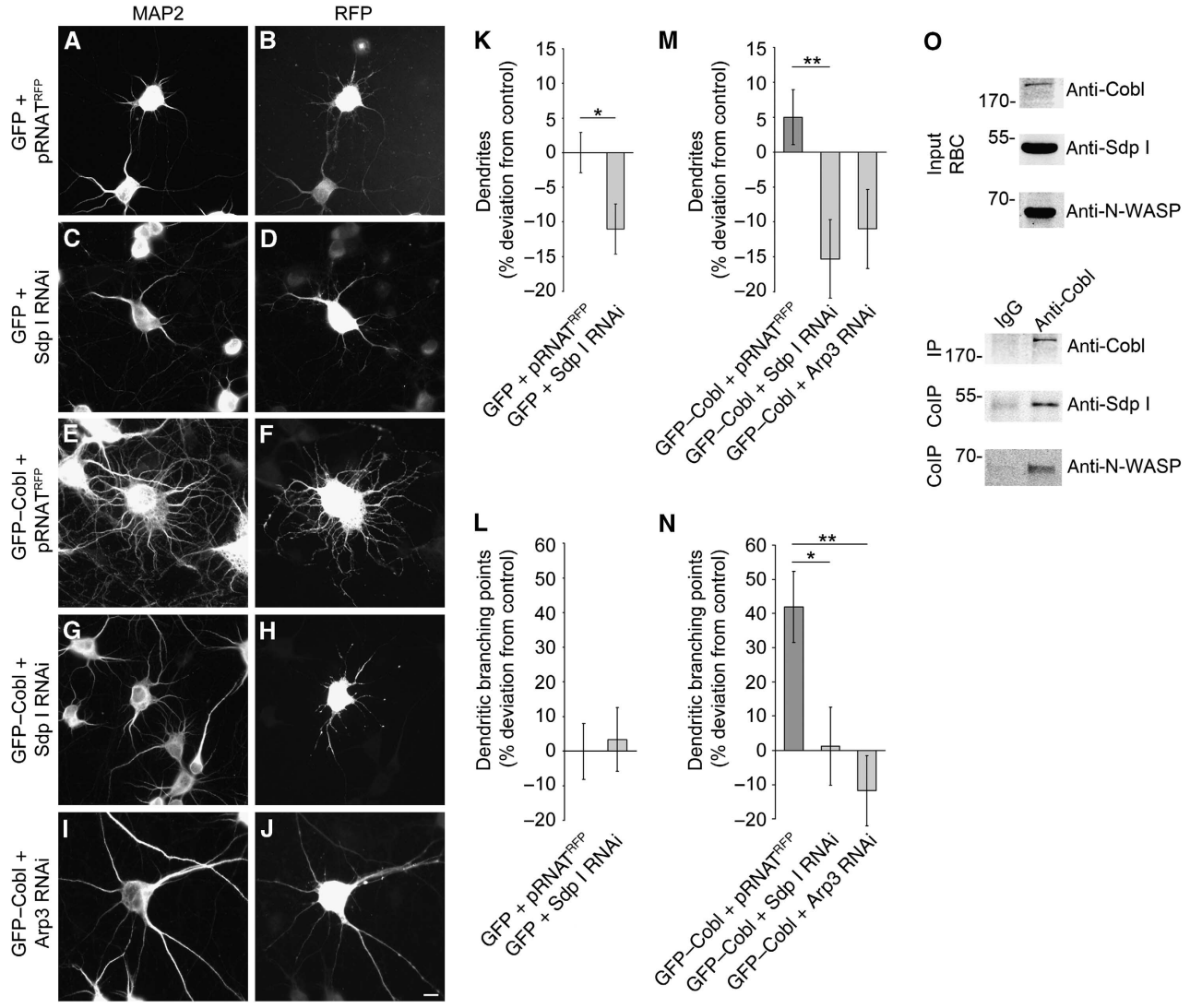

Figure 8 RNAi-based knock down of syndapin I completely suppresses the Cobl-induced increase in dendrite number and dendritic branching. (**A**–**J**) DIV4 primary hippocampal neurons transfected as indicated and processed for immunofluorescence microscopy 2 days later. Staining of MAP2 was used to evaluate the morphology of transfected neurons (**A**, **C**, **E**, **G**, **I**). Syndapin I-deficient neurons (Sdp I RNAi; **C**, **D**) were marked by decreased dendrite numbers compared with control cells. Neurons cotransfected with GFP–Cobl and pRNAT^{RFP} (**E**, **F**) displayed an increase in dendrite formation and dendritic branching. Both of these Cobl-induced phenotypes were completely abolished upon syndapin I RNAi (**G**, **H**) and Arp3 RNAi (**I**, **J**), respectively. Scale bar, 10 μm. (**K**, **L**) Quantitative evaluations of dendrite numbers (**K**) and dendritic branching points (**L**) of syndapin I-deficient neurons in comparison to control cells show a phenocopy of the 12% reduction in dendrite number reported for Cobl loss-of-function (Ahuja *et al*, 2007). (**M**, **N**) Quantitative evaluations of dendrite numbers and dendritic branching furthermore demonstrate that syndapin I and Arp3 RNAi completely abrogate the Cobl-induced neuromorphogenesis phenotypes. Data represent mean ± s.e.m. GFP and pRNAT^{RFP}, $n=69$; GFP and Sdp I RNAi, $n=90$, GFP–Cobl and pRNAT^{RFP}, $n=46$; GFP–Cobl and Sdp I RNAi, $n=30$. GFP–Cobl and Arp3 RNAi, $n=25$. $^{*}P<0.05$; $^{**}P<0.01$ (**K**, **L**, *t*-test; **M**, **N**, ANOVA and HSD). (**O**) Immunoprecipitation of endogenous Cobl from rat brain extracts by anti-Cobl antibodies coimmunoprecipitates both syndapin I and N-WASP in a specific manner, as demonstrated by immunoblotting anti-Cobl and IgG immunoprecipitates with anti-Cobl, anti-syndapin I and anti-N-WASP antibodies.

(Ahuja *et al*, 2007). Provided that the Cobl/syndapin I complexes we identified are crucially involved in dendritogenesis and are disrupted by reduction of syndapin I expression levels, syndapin I RNAi may lead to defects in dendrite formation. We therefore knocked down syndapin I expression levels in DIV4 neurons using an established RNAi construct (Dharmalingam *et al*, 2009) and analysed their morphology 2 days later. Whereas dendrite branching was unchanged, syndapin I RNAi led to a significant reduction of dendrites compared with control cells (Figure 8A–D, K and L). With −11% (Figure 8K), the observed drop in dendrite numbers was very similar compared with that observed upon Cobl RNAi (−12%; Ahuja *et al*, 2007). Thus, syndapin I deficiency phenocopied the Cobl knockdown effect and led to a similarly reduced dendrite number.

The Cobl-mediated increase in dendrite formation and dendritic branch formation is dependent on syndapin I

Since syndapin I deficiency was able to phenocopy the dendrite reduction observed upon Cobl RNAi, we next asked whether the increases in dendrite number and branching mediated by an excess of Cobl would be dependent on syndapin I. The increases in dendrite branching and dendrite number were both very effectively suppressed by coexpres-

sion of syndapin I RNAi. The fact that Cobl/syndapin I RNAi-expressing cells were not different from syndapin I RNAi-expressing cells showed that suppression of both Cobl phenotypes by syndapin I RNAi was complete (Figure 8G, H, M and N).

The Cobl-mediated functions in dedritogenesis are dependent on the Arp2/3 complex and syndapin I physically links Cobl and the Arp2/3 complex activator N-WASP in vivo

Syndapin I controls Arp2/3 complex-mediated actin nucleation in neuromorphogenesis (Dharmalingam *et al*, 2009). This raised the exciting possibility that, while mechanistically, actin nucleation mediated by Cobl and by the Arp2/3 complex is independent from each other (Ahuja *et al*, 2007), syndapin I may join Cobl- and Arp2/3 complex-mediated actin nucleation during the physiological process of dendritic arbor development. Indeed, knocking down Arp3 using established RNAi tools (Haeckel *et al*, 2008) led to suppression of both Cobl overexpression phenotypes, suggesting that both cellular machines cooperate to bring about the drastic cell morphology changes induced by Cobl (Figure 8I, J, M and N).

Mechanistically, the similar effects of syndapin I and Arp3 RNAi may most easily be explained by a physical connection of Cobl and the Arp2/3 complex activator N-WASP, with whom syndapin I associates and functionally interacts (Qualmann *et al*, 1999; Kessels and Qualmann, 2002; Dharmalingam *et al*, 2009), by syndapin I dimerization (Kessels and Qualmann, 2006). In order to directly address this in brain material, we conducted coimmunoprecipitation studies with anti-Cobl antibodies. The antibodies were indeed able to specifically and effectively immunoprecipitate Cobl from rat brain extracts (Figure 8O). Examinations of the coimmunoprecipitates with anti-syndapin I and anti-N-WASP antibodies revealed that both proteins were specifically coprecipitated by anti-Cobl antibodies (Figure 8O; CoIPs).

Our data thus show that Cobl interacts with syndapin I *in vitro* and *in vivo*, that syndapin I functions as a critical factor in the targeting of Cobl to the cell cortex by direct Cobl/syndapin interactions and syndapin/lipid interactions, that syndapin I thereby is crucial for Cobl-mediated cell morphological changes and that syndapin I furthermore has a role in Cobl-mediated cell morphology alterations by physically interconnecting the actin nucleator Cobl with N-WASP/Arp2/3 complex-driven actin nucleation in nerve cells.

Discussion

The complex architecture of neuronal networks and the extreme connectivity of cells within these networks is a basis for the function and abilities of vertebrate brains. Whereas the role of the Arp2/3 complex during the induction and development of the delicate morphology of neuronal cells is emerging (Strasser *et al*, 2004; Pinyol *et al*, 2007; Shakir *et al*, 2008; Dharmalingam *et al*, 2009; Tahirovic *et al*, 2010), the mechanisms WH2 domain-based nucleators use for spatial control are largely unclear. Here, we show that syndapin I is able to associate with the N-terminal Cobl homology domain of the actin nucleator Cobl, that Cobl/syndapin I complex formation promotes efficient membrane association of Cobl and that such complexes control neuronal morphogenesis.

Coprecipitation and heterologous as well as endogenous coimmunoprecipitation have shown that syndapins bind to Cobl and that the association is mediated by the Cobl N-terminus and the C-terminal syndapin SH3 domain. Syndapin proteins bind to lipid surfaces via their N-terminal domain, the F-BAR domain (Itoh *et al*, 2005; Dharmalingam *et al*, 2009; Wang *et al*, 2009). This leaves the C-terminal SH3 domain free for further interactions. The lipid specificities of syndapins promote binding to the plasma membrane (Itoh *et al*, 2005; Dharmalingam *et al*, 2009). In line with this, endogenous syndapin I indeed associates with the plasma membrane, as demonstrated by density gradient fractionations, and syndapin was able to promote membrane association of Cobl in a F-BAR and SH3 domain-dependent manner. In line with Cobl being recruited to the plasma membrane by syndapin I, endogenous Cobl was also present in the plasma membrane fraction and localized to the cell cortex in neurons. Also, efficient recruitment of Cobl to membranes by syndapin I was directly visualized in living cells by *in vivo* reconstitutions of Cobl/syndapin complexes at defined cellular membranes. Furthermore, studies in neurons revealed that syndapin I RNAi leads to an impairment of Cobl localization at the cell cortex.

Purified recombinant, full-length syndapin proteins used as a probe in blot overlay assays successfully detected Cobl proteins. Thus, Cobl/syndapin complexes are formed by direct interactions. This is in line with the nature of the interaction. SH3 domains usually bind short proline-rich peptide sequences, which contain a PxxP-core, as found in many variations in the proline-rich Cobl N-terminal domain. Within the N-terminal region of Cobl annotated as Cobl homology domain, *in silico* analyses revealed three short proline-rich repeats of unknown function (Carroll *et al*, 2003). Here, we show that these repeats represent binding sites for the SH3 domain of syndapins. All three motifs individually bind to syndapin effectively. The consensus of all three motifs in murine Cobl is KrRAPpPP, a class I motif (Feng *et al*, 1994; Lim *et al*, 1994). All three KrRAPpPP-motifs are highly conserved in Cobl proteins of other species. The high conservation and the fact that syndapin I did not interact with further proline-rich regions in Cobl show that the syndapin I SH3 domain prefers a certain binding consensus and thus exhibits specificity. Importantly, also KrRAPpPP-motifs apparently exhibit specificity for syndapins, as seen from the coprecipitation studies.

Single copies of motifs somewhat similar to the KrRAPpPP-motifs of Cobl can be identified in the PRDs of N-WASP and dynamin I (our unpublished data). Both proteins are further major syndapin I SH3 domain interaction partners in neurons (Qualmann *et al*, 1999; Kessels and Qualmann, 2002, 2006). In dynamin I, the KrRAPpPP-like motif (RRAPAVP) is located in the syndapin I binding, C-terminal PRD (Qualmann *et al*, 1999) and is indeed part of the mapped syndapin I binding site (Anggono and Robinson, 2007). Also in N-WASP, the KrRAPpPP-like motif (RRQAPPPP) is part of the PRD demonstrated to be the syndapin-binding domain (Kessels and Qualmann, 2002).

Together with the fact that syndapins dimerize via self-association of their N-terminal F-BAR domain and additionally may form even larger, lipid-associated lattices upon F-BAR-mediated self-assembly of these dimeric building blocks (Kessels and Qualmann, 2006), this might promote the

efficient formation of membrane-associated multiprotein complexes linking Cobl to a second Cobl protein or to another syndapin I SH3 domain binding partner and thus create larger protein complexes controlling and steering Cobl functions in different physiological processes. This hypothesis was confirmed experimentally by our coimmunoprecipitations of endogenous Cobl, syndapin I and the Arp2/3 complex activator N-WASP in one complex and the finding that the Cobl overexpression phenotype critically involves both the direct interaction partner syndapin I and Arp2/3 complex functions.

The ability of syndapin I to form lipid-associated lattices upon self-assembly provides an elegant mechanism for locally enriching actin nucleators at the plasma membrane. Interestingly, the WH2 domain-containing nucleator Spire has recently been revealed to occur in a dimeric complex with a formin dimer (Quinlan *et al*, 2007). It is conceivable that such arrangements are more generally employed to increase the local concentration of actin nucleators and to make sure that, at a given location, a critical level of actin filament formation is reached to overcome the forces counteracting changes of membrane topology. Using their N-terminal F-BAR domain syndapins provide a curved lipid-binding interface and even have the ability to bend and tubulate membranes they associate with (Itoh *et al*, 2005; Dharmalingam *et al*, 2009; Wang *et al*, 2009). This may help to preferentially recruit syndapin complexes to sites of membrane curvature or promote such curvatures upon syndapin association. Such discontinuities in membrane topology may serve as initiation sites for actin filament-driven, protrusive structures, such as those triggered by both Cobl and syndapin I during dendritic arbor formation. As to be expected for a component recruiting Cobl to the cell cortex, syndapin I coexpression promoted the Cobl phenotype. Strong evidence that the similarity of the syndapin I and the Cobl gain-of-function phenotypes is not just a coincidence and the strong effect on dendritogenesis upon Cobl/syndapin I coexpression is not just due to parallel pathways is provided (i) by the finding that Cobl/syndapin complexes occur in the brain, (ii) by the fact that deficiency of syndapin I and Cobl in DIV6 neurons led to comparable reductions of dendrite numbers and (iii) most importantly, by the observation that Cobl-mediated functions are critically dependent on its interaction partner syndapin I. The observation that syndapin I is not required for dendritic branching although syndapin I RNAi can completely suppress branching induced by Cobl overexpression indicates that, while syndapin I can be used to promote branching, as also seen from the syndapin I overexpression phenotype (Dharmalingam *et al*, 2009), other factors may be partially functionally redundant with syndapin I in this physiological process.

Whether the proposed early embryonic function of Cobl in neurotube closure and body axes formation, which is based on the specific detection of Cobl mRNA in the gastrula organizer and the axial midline in the forming embryo and genetic interactions with the gene Vangl2 (Gasca *et al*, 1995; Carroll *et al*, 2003), also relies on syndapin I, is currently not to be answered but seems somewhat unlikely. Syndapin I expression is still relatively low during early embryonic development (Dharmalingam *et al*, 2009). Possible, however, is an involvement of syndapin II and/or III in early embryonic development. Our analyses demonstrate that these proteins also associate with Cobl, and syndapin III has recently been shown to have a critical role in embryonic notochord development in zebrafish (Edeling *et al*, 2009).

With the findings that Cobl is interacting with syndapin I, that both proteins work together in dendritogenesis, that syndapin I is a crucial factor in Cobl-mediated functions in neuromorphogenesis, that these functions are brought about by direct syndapin I interaction with a highly conserved triplet of syndapin-binding consensus motifs used to define the thus far uncharacterized Cobl homology domain and that syndapin I is important for the membrane recruitment of the actin nucleator Cobl, this study reveals important molecular mechanisms for the spatial control of the actin nucleator Cobl in neuronal cells and for how it is interconnected to N-WASP/Arp2/3 complex functions in neuromorphogenesis. Our examinations thereby help to shed light on how neuronal cells use actin nucleators to steer the complex cytoskeletal reorganizations underlying neuronal shape modulation and the formation of neuronal networks—prerequisites for proper brain development and neuronal cell–cell communication.

Materials and methods

DNA constructs and recombinant proteins

For detailed description of plasmids and purification procedures for recombinant fusion proteins please see the Supplementary data.

Antibodies

Affinity-purified rabbit and guinea pig anti-syndapin I, rabbit anti-syndapin II and anti-GST antibodies were described previously (Qualmann *et al*, 1999; Qualmann and Kelly, 2000; Braun *et al*, 2005).

Anti-Cobl antibodies were raised against HisTRX-tagged Cobl 175–324Δ262–286 (ARA) and 750–1005 (DBY) in rabbits and guinea pigs. Sera were affinity purified against immunoblotted GST-tagged fusion proteins according to the procedures described previously (Qualmann *et al*, 1999). Additionally, anti-HisTRX antibodies were affinity purified from the same sera using immobilized HisTRX protein.

Sera and all affinity-purified antibodies were tested in western blot analyses with different amounts of recombinant antigen, GFP–Cobl-expressing HEK293 cell and rat brain lysates, respectively. Additionally, the antibodies were characterized by immunofluorescence studies of COS-7 cells expressing Cobl constructs.

Commercially available primary and secondary antibodies are listed in the Supplementary data.

Preparation and fractionation of HEK293 cell and brain extracts

Transfected and nucleofected HEK293 cells, respectively, were harvested and lysed in 10 mM HEPES pH 7.4, 1 mM EGTA, 0.1 mM $MgCl_2$, 1% Triton X-100 (lysis buffer) supplemented with 100 or 150 mM NaCl and protease inhibitor Complete® EGTA-free (Roche) 48 h after transfection. Supernatants obtained by centrifugation at 20 000 *g* were used for coprecipitation and coimmunoprecipitation experiments.

Lysates for coimmunoprecipitation of endogenous proteins were prepared from brains of 8-week-old male rats homogenized in lysis buffer (1:3 (w/v)). Lysis buffers were supplemented with 50 mM NaCl and 40 mM NaCl and 1 mM DTT, respectively, as well as with protease inhibitor. Rat brain extracts were prepared using an Ultra Turrax homogenizer at 20 000 r.p.m. for 10 s and centrifugation at 150 000 *g* for 45 min or 100 000 *g* for 1 h.

Subcellular fractionation and floatation assays

Rat cerebrum was homogenized in ice-cold lysis buffer with 150 mM NaCl and protease inhibitor (1:3 (w/v)) using a Potter S homogenizer. In all, 525 µl lysate was supplemented with 175 µl of 1 M sucrose in PBS and centrifuged at 1000 *g* (3 min at 4°C). The resulting supernatant was subjected to floatation assays according to Kretzschmar *et al* (1996). A volume of 200 µl of the supernatant was diluted to 1 ml by adding sucrose (68.5% final), placed under

two cushions of 65% (7 ml) and 10% sucrose (10 ml) and centrifuged overnight at 4°C at 175 000 *g*. Fractions of 1 ml were collected from top to bottom. The lower 12 fractions obtained were ethanol precipitated and immunoblotted.

Coprecipitation and blot overlay analyses

Coprecipitations of GFP–Cobl fusion proteins expressed in HEK293 cells were conducted with 30 μg of purified GST fusion proteins immobilized on 25 μl of glutathione sepharose beads, as described previously (Qualmann *et al*, 1999). Bound proteins were eluted with 10 mM reduced glutathione, 50 mM Tris/HCl pH 8.0, separated by SDS–PAGE and analysed by anti-GFP immunoblotting. Alternatively, bound proteins were obtained by boiling the beads in 4 × SDS sample buffer.

For analysis of proteins associating with GST–Cobl 318–332 (KrRAPpPP-motif #2), rat brain extracts were incubated with 125 μg fusion protein attached to 0.2 ml resin bed glutathione spin columns (Pierce), incubated for 3 h and eluted three times with 200 μl 20 mM reduced glutathione in 50 mM Tris/HCl, 120 mM NaCl, pH 8. The eluates were precipitated overnight with acetone (1:4), centrifuged at 10 000 *g* for 30 min and resolved in 50 μl SDS sample buffer, separated via SDS–PAGE and finally stained with Coomassie and subjected to immunoblotting, respectively. In control experiments, brain extracts were omitted.

All affinity purifications were accompanied by control experiments with GST attached to the beads. Integrity of GST fusion proteins (reisolated by boiling the beads in 4 × SDS sample buffer) was analysed by SDS–PAGE and Coomassie or Ponceau staining and anti-GST immunoblotting, respectively.

Blot overlay experiments were performed on blotted HEK293 cell lysates containing different GFP–Cobl fusion proteins with purified GST-tagged syndapin I, II and III fusion proteins as probes (Kessels and Qualmann, 2002). Bound protein probes were detected by anti-GST antibodies.

Heterologous and endogenous coimmunoprecipitations

For heterologous immunoprecipitations, 1.5 μg monoclonal anti-Flag antibody (M2) and 2 μg non-immune mouse IgG (Santa Cruz) were coupled to protein A agarose (Santa Cruz) in PBS containing 5% (w/v) BSA, washed with lysis buffer supplemented with 100 mM NaCl and incubated overnight with HEK293 cell extracts containing Flag-syndapins and different GFP–Cobl constructs. After washing the resin with the above buffer, bound proteins were eluted with 4 × SDS sample buffer and subjected to immunoblotting analyses with anti-syndapin I, anti-syndapin II and anti-GFP antibodies.

Endogenous Cobl/syndapin I complexes were immunoprecipitated from rat brain extracts using rabbit anti-syndapin I antibodies and endogenous Cobl/syndapin I/N-WASP complexes were immunoprecipitated with rabbit anti-Cobl (ARA) antibodies. The antibodies and unrelated rabbit IgGs, respectively, were immobilized to protein A agarose in the presence of 5% BSA and incubated with 1 mg rat brain protein each. Immunoprecipitates were washed, eluted with 4 × SDS sample buffer and analysed by immunoblotting with guinea pig anti-syndapin I, rabbit anti-Cobl antibodies and guinea pig anti-N-WASP antibodies, respectively.

Liposome-binding assays

Liposomes were made of lipids from Folch-fraction type I, as described (Reeves and Dowben, 1969), and resuspended in 0.3 M sucrose. In all, 200 μg liposomes were incubated with 1 μM purified recombinant protein and protein complexes isolated by coprecipitation from lysates of transfected HEK293 cells respectively, in 25 mM HEPES-KOH pH 7.2, 25 mM KCl, 2.5 mM magnesium acetate and 100 mM potassium glutamate (cytosol buffer) for 15 min at 37°C. Final volumes of 100 μl were then mixed with 150 μl 75% sucrose to yield a final sucrose concentration of 45%. The mixture was overlayed with 200 μl 35% sucrose and 200 μl cytosol buffer and centrifuged at 200 000 *g* for 30 min at 28°C. Six 100 μl fractions were collected from top to bottom and analysed by SDS–PAGE and immunoblotting with anti-GST and anti-Cobl antibodies. Quantitative analyses were conducted using fluorescently labelled antibodies and a Licor Odyssey System. Statistical analysis was performed using the two-tailed Student's *t*-test.

The liposome-containing fractions were identified in control experiments with liposomes dotted with 5% of Rhodamine B-conjugated phosphatidylethanolamine (Avanti polar lipids; Sigma) (Dharmalingam *et al*, 2009).

Brain sectioning and immunolabelling of mouse brain sections

Mice were anaesthesized by abdominal injections of 300 μl of a mixture composed of 72 μl ketamine hydrochloride (50 mg/ml), 25.5 μl Rompun (2% injection solution) and 202.5 μl 0.9% (w/v) NaCl and perfused through the left ventricle with PBS and thereafter with 4% PFA in PBS.

Brains were removed, postfixed in 4% paraformaldehyde for 16 h at 4°C, rinsed with PBS and tap water, and then placed in 30% (w/v) sucrose in PBS at 4°C until they sank. Brains were sliced sagittally on a sliding microtome (SM 2000R; Leica) at 55 μm. Slices were collected in multiwell plates containing PB (77.4 mM Na_2HPO_4, 22.6 mM NaH_2PO_4), were swayed in PB (2 × 5 s) and then permeabilized and blocked with 5% (v/v) goat serum, 0.25% (v/v) Triton X-100 in PB (block solution) for 2 h at RT. For labelling with primary antibodies, slices were incubated with 300 μl antibody in block solution for 48 h at 4°C. The slices were washed 3 × with PB and subsequently incubated with secondary antibody conjugates for 16 h at 4°C. Nuclei were labelled by incubation with DAPI (1:1000 in PB) for 30 min. Thereafter, slices were transfered into PBS and mounted with Fluoromont-G™ onto HistoBond® slides and sealed with nail polish.

Cell culture and processing for immunofluorescence

Culturing of HEK293 and COS-7 cells as well as preparation and maintenance of primary hippocampal neurons was done according to published standard procedures (also see Supplementary data for further information).

Microscopy

Images were recorded using a Zeiss AxioObserver.Z1 microscope or a Zeiss AxioImager.D1 both equipped with Zeiss Plan-Apochromat 63 × /1.4 and 40 × /1.3 objectives. The microscopes were connected to an AxioCam MRm CCD camera (Zeiss) and a CCD camera 2.1.1 (Diagnostic Instruments), respectively. Confocal imaging was done by using a Zeiss AxioObserver equipped with an ApoTome and by employing a Leica TCS NT laser confocal microscope, respectively. Digital images were recorded by SpotSoftware and AxioVision, respectively, and processed by ImageJ or Adobe Photoshop.

Subcellular Cobl localization was quantitatively determined using plot profiles across cells (ImageJ) from three independent assays. To distinguish cortical from more internal immunosignals, the maximal fluorescence intensities of the flanking peaks (cortex value) and the intensities of all pixels between the two cell cortex peaks were averaged (cytosol value). To account for putative differences in labelling intensities, the differences between cells transfected with PM-GFP (marker) and with syndapin I RNAi and PM-GFP, respectively, were expressed as ratios of cortical/cytosolic signal. Statistical analysis was performed using the two-tailed Student's *t*-test.

Morphometric analyses of primary hippocampal neurons

Morphometric measurements and knockdown intensity measurements of transiently transfected hippocampal neurons were performed with ImageJ according to Ahuja *et al* (2007); Pinyol *et al* (2007); and Dharmalingam *et al* (2009). Each experiment was repeated 2–7 times with independent neuronal preparations. The number of dendrites and the number of dendritic branching points were determined from 25 to 220 DIV6 neurons for each condition. A minimal length of 10 μm was used as cutoff for the evaluation of dendritic branches. All data were normalized to the corresponding controls run in parallel in each individual experiment and neuronal preparation. Statistical analysis was performed using the two-tailed Student's *t*-test and one-way analysis of variance (ANOVA) followed by Tukey's honestly significant difference (HSD) test, respectively.

Supplementary data

Supplementary data are available at *The EMBO Journal* Online (http://www.embojournal.org).

Acknowledgements

We thank D Schlobinski for his help and M Öhler and A Kreusch for their excellent technical assistance. This work was supported by grants from the DFG to BQ (Qu116/5-1, 6-1), to MMK (KE685/2-3, 3-1) and to both (Qu116/3-3 and 7-1), respectively, as well as by a grant from the Schram-Foundation (T287/16245/2006).

Author contributions: LS, NK, RA and JG performed the experiments. LS, NK, RA, JG, MMK and BQ analysed and discussed the data; MMK and BQ supervised the studies and wrote the paper.

Conflict of interest

The authors declare that they have no conflict of interest.

References

Ahuja R, Pinyol R, Reichenbach N, Custer L, Klingensmith J, Kessels MM, Qualmann B (2007) Cordon-bleu is an actin nucleation factor and controls neuronal morphology. *Cell* **131:** 337–350

Anggono V, Robinson PJ (2007) Syndapin I and endophilin I bind overlapping proline-rich regions of dynamin I: role in synaptic vesicle endocytosis. *J Neurochem* **102:** 931–943

Aspenström P (2009) Roles of F-BAR/PCH proteins in the regulation of membrane dynamics and actin reorganization. *Int Rev Cell Mol Biol* **272:** 1–31

Braun A, Pinyol R, Koch D, Dahlhaus R, Fonarev P, Grant BD, Kessels MM, Qualmann B (2005) EHD proteins associate with syndapin I and II and such interactions play a crucial role in endosomal recycling. *Mol Biol Cell* **16:** 3642–3658

Carroll EA, Gerrelli D, Gasca S, Berg E, Beier DR, Copp AJ, Klingensmith J (2003) Cordon-bleu is a conserved gene involved in neural tube formation. *Dev Biol* **262:** 16–31

Chereau D, Boczkowska M, Skwarek-Maruszewska A, Fujiwara I, Hayes DB, Rebowski G, Lappalainen P, Pollard TD, Dominguez R (2008) Leiomodin is an actin filament nucleator in muscle cells. *Science* **320:** 239–243

Chesarone MA, Goode BL (2009) Actin nucleation and elongation factors: mechanisms and interplay. *Curr Opin Cell Biol* **21:** 28–37

Conde C, Cáceres A (2009) Microtubule assembly, organization and dynamics in axons and dendrites. *Nat Rev Neurosci* **10:** 319–332

Dharmalingam E, Haeckel A, Pinyol R, Schwintzer L, Koch D, Kessels MM, Qualmann B (2009) F-BAR proteins of the syndapin family shape the plasma membrane and are crucial for neuromorphogenesis. *J Neurosci* **29:** 13315–13327

Edeling MA, Sanker S, Shima T, Umasankar PK, Höning S, Kim HY, Davidson LA, Watkins SC, Tsang M, Owen DJ, Traub LM (2009) Structural requirements for PACSIN/Syndapin operation during zebrafish embryonic notochord development. *PLoS ONE* **4:** e8150

Feng S, Chen J, Yu H, Simmon J, Schreiber S (1994) Two binding orientations for peptides to the Src SH3 domain: development of a general model for SH3-ligand interactions. *Science* **266:** 1241–1247

Frost A, Perera R, Roux A, Spasov K, Destaing O, Egelman EH, De Camilli P, Unger VM (2008) Structural basis of membrane invagination by F-BAR domains. *Cell* **132:** 807–817

Fütterer K, Machesky LM (2007) 'Wunder' F-BAR domains: going from pits to vesicles. *Cell* **129:** 655–657

Gasca S, Hill DP, Klingensmith J, Rossant J (1995) Characterization of a gene trap insertion into a novel gene, cordon-bleu, expressed in axial structures of the gastrulating mouse embryo. *Dev Genet* **17:** 141–154

Haeckel A, Ahuja R, Gundelfinger ED, Qualmann B, Kessels MM (2008) The actin-binding protein Abp1 controls dendritic spine morphology and is important for spine head and synapse formation. *J Neurosci* **28:** 10031–10044

Itoh T, Erdmann KS, Roux A, Habermann B, Werner H, De Camilli P (2005) Dynamin and the actin cytoskeleton cooperatively regulate plasma membrane invagination by BAR and F-BAR proteins. *Dev Cell* **9:** 791–804

Kessels MM, Qualmann B (2002) Syndapins integrate N-WASP in receptor-mediated endocytosis. *EMBO J* **21:** 6083–6094

Kessels MM, Qualmann B (2004) The syndapin protein family: linking membrane trafficking with the cytoskeleton. *J Cell Sci* **117:** 3077–3086

Kessels MM, Qualmann B (2006) Syndapin oligomers interconnect the machineries for endocytic vesicle formation and actin polymerization. *J Biol Chem* **281:** 13285–13299

Kessels MM, Schwintzer L, Schlobinski D, Qualmann B (2011) Controlling actin cytoskeletal organization and dynamics during neuronal morphogenesis. *Eur J Cell Biol* (advance online publication 19 October 2010; doi:10.1016/j.ejcb.2010.08.011)

Kretzschmar E, Bui M, Rose JK (1996) Membrane association of influenza virus matrix protein does not require specific hydrophobic domains or the viral glycoproteins. *Virology* **220:** 37–45

Lim WA, Richards FM, Fox RO (1994) Structural determinants of peptide-binding orientation and of sequence specificity in SH3 domains. *Nature* **372:** 375–379

Pérez-Otãno I, Luján R, Tavalin SJ, Plomann M, Modregger J, Liu X-B, Jones EG, Heinemann SF, Lo DC, Ehlers MD (2006) Endocytosis and synaptic removal of NR3A-containing NMDA receptors by PACSIN1/syndapin1. *Nat Neurosci* **10:** 611–621

Pinyol R, Haeckel A, Ritter A, Qualmann B, Kessels MM (2007) Regulation of N-WASP and the Arp2/3 complex by Abp1 controls neuronal morphology. *PLoS One* **2:** e400

Qualmann B, Kelly RB (2000) Syndapin isoforms participate in receptor-mediated endocytosis and actin organization. *J Cell Biol* **148:** 1047–1061

Qualmann B, Kessels MM (2009) New players in actin polymerization—WH2 domain-containing actin nucleators. *Trends Cell Biol* **19:** 276–285

Qualmann B, Roos J, DiGregorio PJ, Kelly RB (1999) Syndapin I, a synaptic dynamin-binding protein that associates with the neural Wiskott-Aldrich syndrome protein. *Mol Biol Cell* **10:** 501–513

Quinlan ME, Heuser JE, Kerkhoff E, Mullins RD (2005) Drosophila Spire is an actin nucleation factor. *Nature* **433:** 382–388

Quinlan ME, Hilgert S, Bedrossian A, Mullins RD, Kerkhoff E (2007) Regulatory interactions between two actin nucleators, Spire and Cappuccino. *J Cell Biol* **179:** 117–128

Reeves JP, Dowben RM (1969) Formation and properties of thin-walled phospholipid vesicles. *J Cell Physiol* **1:** 49–60

Shakir MA, Jiang K, Struckhoff EC, Demarco RS, Patel FB, Soto MC, Lundquist EA (2008) The Arp2/3 activators WAVE and WASP have distinct genetic interactions with Rac GTPases in Caenorhabditis elegans axon guidance. *Genetics* **179:** 1957–1971

Strasser GA, Rahim NA, VanderWaal KE, Gertler FB, Lanier LM (2004) Arp2/3 is a negative regulator of growth cone translocation. *Neuron* **43:** 81–94

Tahirovic S, Hellal F, Neukirchen D, Hindges R, Garvalov BK, Flynn KC, Stradal TE, Chrostek-Grashoff A, Brakebusch C, Bradke F (2010) Rac1 regulates neuronal polarization through the WAVE complex. *J Neurosci* **30:** 6930–6943

Wang Q, Navarro MV, Peng G, Molinelli E, Lin Goh S, Judson BL, Rajashankar KR, Sondermann H (2009) Molecular mechanism of membrane constriction and tubulation mediated by the F-BAR protein Pacsin/Syndapin. *Proc Natl Acad Sci USA* **106:** 12700–12705

Zuchero JB, Coutts AS, Quinlan ME, Thangue NB, Mullins RD (2009) p53-cofactor JMY is a multifunctional actin nucleation factor. *Nat Cell Biol* **11:** 451–459